ORGANIC CHEMISTRY FRONTIERS

RESEARCH ARTICLE

View Article Online
View Journal | View Issue

Cite this: *Org. Chem. Front.*, 2026, **13**, 2367

Synergistic experimental and theoretical investigation of carbazole–cyanopyridine-based hole-transporting materials

Rachel Chetri,[a] Vygintas Jankauskas,[b] Gediminas Kreiza,[d] Kasparas Rakstys,[c] Vytautas Getautis,[c] Rahim Ghadari,[e] Arijit Saha[a] and Ahipa Tantri Nagaraja *[a]

This work highlights the design, synthesis, and characterization of three new hole-transporting materials (**DJ01-alkyl**, **PR01-alkyl**, and **PM01-alkyl**) based on donor–acceptor–donor (D–A–D) and acceptor–acceptor–donor (A–A–D) concepts. Crystals of two compounds, **DJ01-alkyl** and **PR01-alkyl**, were obtained under similar crystallization conditions. The molecular structures were thoroughly examined using DFT, photophysical, electrochemical, and thermal methods. The UV-vis absorption spectrum of **DJ01-alkyl** displayed a significant bathochromic effect compared to its counterparts **PR01-alkyl** and **PM01-alkyl**. This could be because the thiophene units enhance conjugation and lead to a bathochromic shift. Compared to **DJ01-alkyl** (1.7×10^{-5} cm^2 V^{-1} s^{-1}) and **PM01-alkyl** (1.6×10^{-5} cm^2 V^{-1} s^{-1}), **PR01-alkyl** was found to have a higher hole mobility value of 2.1×10^{-5} cm^2 V^{-1} s^{-1}. To further explain and complement the experimental data, DFT calculations of the geometry, electronic structure, absorption, reorganization energy, transition density matrix, and density of states of compounds were performed. These characteristics make it abundantly evident that compounds based on carbazoles and cyanopyridines are very attractive materials for use as hole-transporting materials in perovskite solar cells.

Received 20th January 2026,
Accepted 16th February 2026

DOI: 10.1039/d6qo00076b

rsc.li/frontiers-organic

1. Introduction

Research on renewable energy is gaining significance and is increasingly crucial to meet future energy security requirements.[1] Since clean energy is abundant in nature, different types of solar cells have gained international interest as renewable energy sources. Perovskite solar cells (PSCs) have garnered a lot of attention from researchers in recent years due to their low cost and sharp rise in efficiency, which has increased from 3.8% in 2009 to 27.0% to date.[2–5] A perovskite absorber is sandwiched between an electron-transporting material (ETM) and a hole-transporting material (HTM) in a typical PSC.[6,7] HTMs play an important role in PSCs in extracting holes from the perovskite layer to the metal electrode and also help in device stability.[2,8] A desirable HTM should be able to form films, have high hole mobility, good solubility, and the right frontier molecular orbitals. Hence, 2,2′,7,7′-tetrakis-(*N*,*N*-di-*p*-methoxyphenylamine)9,9′-spirobifluorene (Spiro-OMeTAD) is the most widely used HTM in PSCs, despite its low charge carrier mobility and low-yield production, which severely limit its widespread use.[9–11] The benefits of Spiro-OMeTAD include the capacity to sustain a stable amorphous state and an excellent energy level match between the perovskite absorber and this HTM's highest occupied molecular orbital (HOMO).[12] Due to the poor conductivity and mobility of pristine Spiro-OMeTAD films, dopants like 4-*tert*-butylpyridine (TBP) and lithium bis(trifluoromethylsulfonyl)imide (Li(TFSI)) are used. These dopants make PSCs unstable because of their hygroscopic properties.[13–15] Therefore, dopant-free HTMs, such as metal complexes,[16,17] conjugated polymers,[18,19] small organic molecules,[20,21] and inorganic compounds,[22] have been investigated and used in PSCs in place of Spiro-OMeTAD. In general, the HOMO level of an HTM needs to be well aligned with the valence band of perovskites in order to enable an efficient hole injection from the perovskite to the HTM.[23–27]

The advantages of carbazole-based HTMs include the low cost and availability of the 9*H*-carbazole precursor and its derivatives, strong electron-donating ability, suitable energy level alignment, and excellent chemical and environmental

[a]*Centre for Nano and Material Sciences, Jain (Deemed-to-be University), Jain Global Campus, Kanakapura, Bangalore, Karnataka-562112, India. E-mail: tn.ahipa@jainuniversity.ac.in*
[b]*Institute of Chemical Physics, Vilnius University, Saulėtekio al. 3, 10257 Vilnius, Lithuania*
[c]*Department of Organic Chemistry, Kaunas University of Technology, Radvilenu pl. 19, Kaunas 50254, Lithuania*
[d]*Institute of Photonics and Nanotechnology, Vilnius University, Saulėtekio al. 3, 10257 Vilnius, Lithuania*
[e]*Computational Chemistry Laboratory, Department of Organic and Biochemistry, Faculty of Chemistry, University of Tabriz, Tabriz 5166616471, Iran*

stability arising from the fully aromatic framework. Moreover, the structural versatility of carbazole allows for facile modification through the incorporation of various alkyl or functional groups at the nitrogen atom or on the outer benzene ring, enabling precise tuning of optoelectronic properties, solubility, and molecular packing behavior.[28–31]

Numerous investigations have also demonstrated that pyridine units can efficiently passivate interface defects and improve the capacity to extract and transport holes.[32] The pyridine moiety can function as a Lewis base, which helps with the π-conjugation and therefore prevents the defect passivation of the perovskite.[33–36] It was reported by Xu *et al.*[35] that compared to Spiro-OMeTAD-based solar cells with TBP added, PSCs with pyridine functionalized HTMs demonstrated significantly higher long-term stability. Also, Duan *et al.*[37] have reported that the cyano (CN) group has been used extensively as a stronger acceptor in D–A type conjugated small molecules as dopant-free HTMs for high-performing PSCs because of its high hole-mobility and structural variety. Numerous other organic electronics applications, including OSCs, OLEDs, electrochromic and photochromic windows, and sensors, have had success with thiophene derivatives. Thiophene derivatives have been used as HTMs in PSCs due to their many potential uses, high chemical stability, superior electrical configuration, and remarkable synthetic diversity. In actuality, thiophene-based HTMs benefit from their electron-rich thiophene cores, which raise the rate at which charges self-exchange.[38,39] Additionally, organic HTMs carrying nitro and bromo groups have been employed in PSCs.[40,41] The tunable optical and electrical features of D–A–D type conjugated molecules make them some of the most intriguing systems.[42,43] Furthermore, the A–A–D system often shows a strong dipole–dipole interaction, which may help with molecular packing and enhance the hole transport capacity.[44,45] Additionally, alkyl chains, which are often introduced to enhance the solubility of HTMs, also play a crucial role in improving device performance by influencing molecular packing and film morphology.[45] Long alkyl chains are also known to create an insulating layer during interface engineering and help to reduce electron recombination and increase the V_{oc}.[46] Thus, it has been found that the solubility of HTMs in organic solvents and, consequently, the molecular ordering during the spin coating process are influenced by the length of the alkyl chains as reported by Zhang *et al.*[47] Also, addition of a hexyl chain into a carbazole molecule enhances the carbazole moiety's spatial hindrance, making it suitable for producing thin and amorphous layers with a suitable morphology on substrates.[48,49]

In this work, we have synthesized three new carbazole and cyanopyridine based HTMs termed **DJ01-alkyl** (thiophenyl), **PR01-alkyl** (4-bromophenyl), and **PM01-alkyl** (4-nitrophenyl), new simple carbazole-based HTMs containing cyanopyridine as a core moiety (Scheme 1 illustrates their chemical structures). Among them, **DJ01-alkyl** possesses a D–A–D type molecular architecture, whereas **PR01-alkyl** and **PM01-alkyl** possess a A–A–D configuration. In recent years, thiophene-based derivatives have gained significant attention as HTMs in PSCs owing to their excellent performance, low cost, and high reliability.[39] Moreover, organic HTMs bearing bromo and nitro substituents have also been explored in PSCs, demonstrating promising performance and tunable electronic properties.[40,41] Thus, our research sheds light on the viability of modifying the donor units to achieve dopant-free HTMs in addition to offering logical design guidelines for effective HTMs.

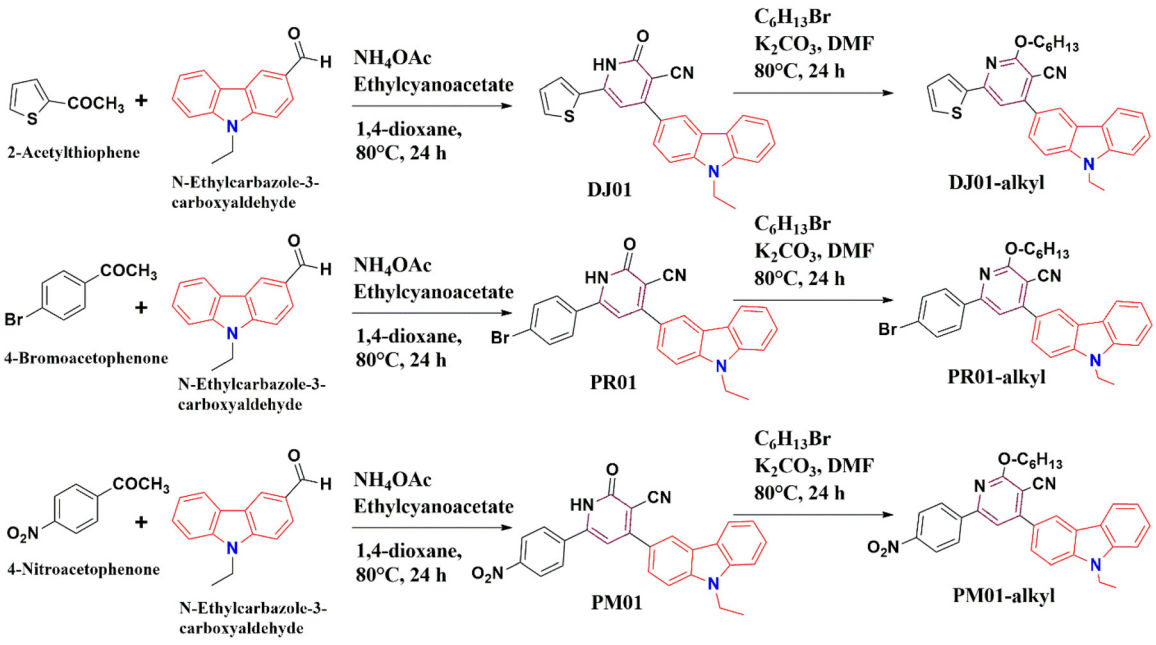

Scheme 1 The synthesis of **DJ01-alkyl**, **PR01-alkyl**, and **PM01-alkyl**.

2. Results and discussion

2.1 Materials synthesis

Scheme 1 gives the detailed synthesis of the three new molecules, **DJ01-alkyl**, **PR01-alkyl**, and **PM01-alkyl**, with yields of 64–72%. DJ01, PR01 and PM01 were synthesized using a mixture of *N*-ethylcarbazole-3-carboxyaldehyde, which was kept constant, and other reactants that were varied, like 2-acetylthiophene (DJ01), 4-bromoacetophenone (PR01), and 4-nitroacetophenone (PM01), which was already reported in our previous work.[50] DJ01, PR01, and PM01 exhibit limited solubility in common organic solvents, which poses challenges for solution processing and detailed characterization. Therefore, alkylation was intentionally carried out as a molecular design strategy to enhance solubility. The introduction of alkyl substituents increases the hydrophobic character and conformational flexibility of the molecules, weakens strong intermolecular interactions such as π–π stacking, and reduces molecular planarity. As a result, the alkylated derivatives show improved solubility in conventional organic solvents (Table S5), facilitating good hole mobility. ^{1}H NMR spectroscopy shows the formation of alkylated products by typical chemical shifts of the alkyl group of about 1–4.5 ppm, were used to correlate the chemical structures of all three compounds. The SI provides a detailed synthesis process (S4–S13). The compounds exhibit good solubility in a variety of common organic solvents, including dichloromethane, chloroform, tetrahydrofuran, chlorobenzene, and toluene. The SI provides a thorough cost estimate and synthesis processes for the production of compounds. The costs for synthesizing **DJ01-alkyl**, **PR01-alkyl**, and **PM01-alkyl** (including reagents, solvents, and other consumables) were calculated to be just \$11.41, \$11.90, and \$11.79 per g (Tables S1, S2, and S3), respectively, which are markedly lower than that of the benchmark HTM, Spiro-OMeTAD (\$400 per g).[51] A summary of the cost calculations of various carbazole based HTMs is shown in Table S4. This suggests a viable approach for commercial production scale-up.

Among the three synthesized molecules, we were able to get single crystals for **DJ01-alkyl** and **PR01-alkyl**. Single crystals were grown from chlorobenzene solvent at room temperature. The chemical structures of **DJ01-alkyl** and **PR01-alkyl** were confirmed by X-ray diffraction analysis as displayed in Fig. 1a and b. Furthermore, a single-crystal study reveals that **DJ01-alkyl** crystallises in the monoclinic space group $P2_1/c$ with cell parameters a = 20.0534(5) Å, b = 11.8621(3) Å, c = 10.8047(2) Å, V = 2567.70(10) Å^3, and Z = 4, whereas **PR01-alkyl** crystallises in the monoclinic space group $C2/c$ with cell parameters a = 42.0517(6) Å, b = 7.42350(10) Å, c = 18.4826(3) Å, V = 5737.19 (15) Å^3, and Z = 8 (Table S6). Furthermore, single crystal structure analysis reveals that for both the molecules the centre moiety (cyanopyridine), the carbazole moiety and the remaining moieties thiophenyl (**DJ01-alkyl**) and 4-bromophenyl (**PR01-alkyl**) do not lie in the same plane. In the case of the **PR01-alkyl** moiety the dihedral angle between 4-bromophenyl

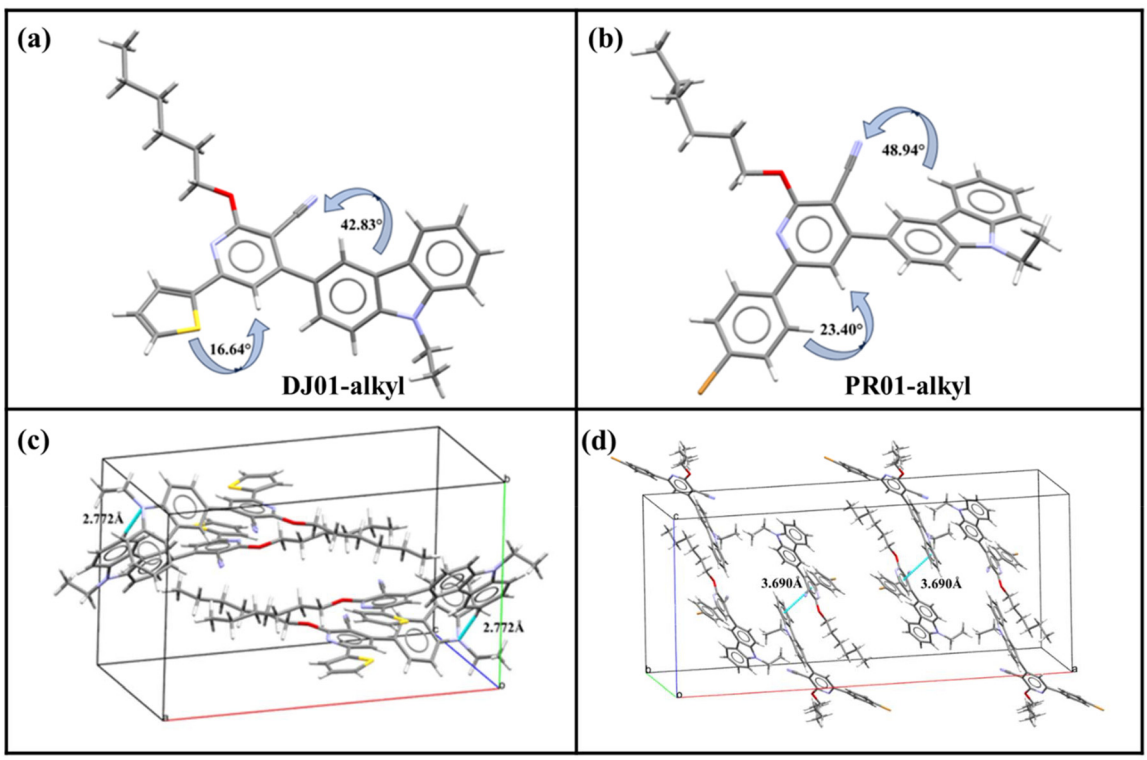

Fig. 1 Single-crystal structures of (a) **PR01-alkyl** and (b) **DJ01-alkyl**; and (c) N···H interactions in **DJ01-alkyl** and (d) π–π interactions with distances in **PR01-alkyl**.

and cyanopyridine is 23.40°, while the dihedral angle between the carbazole and cyanopyridine is 48.94°. On the other hand, for the **DJ01-alkyl** moiety the dihedral angle between cyanopyridine and the thiophenyl ring is 16.64° and the dihedral angle between carbazole and cyanopyridine is 42.83°. Thus, the thiophenyl ring is almost planar with the cyanopyridine ring in the **DJ01-alkyl** moiety, which helps it to transfer the charge through the ring, and this results in a bathochromic shift in the emission.[52,53] Also, in the crystal structure we observed N···H interactions (2.772 Å) which help this charge transfer (Fig. 1c). Furthermore, we can observe π–π interactions in the **PR01-alkyl** moiety (Fig. 1d), where the π–π interaction distance in the crystal structure is 3.690 Å, which is well within the range for π–π interactions.[54] These π–π interactions play a crucial role in the hole mobility of the **PR01-alkyl** moiety.[55] Therefore, we calculated the interaction energy of the π–π conjugated molecular pair of the **PR01-alkyl** moiety by using Crystal Explorer (CE) software.[56] Furthermore, the interaction energy calculated from CE also indicates the presence of π–π interactions, which results in high dispersion energy in the **PR01-alkyl** moiety pair (−87.3 kJ mol^{-1}).

2.2 Photophysical and electrochemical properties

Fig. 2a displays the UV-vis absorption and fluorescence emission spectra of **DJ01-alkyl**, **PR01-alkyl**, and **PM01-alkyl**, and Table 1 summarizes the characteristic data. The absorption spectra show that **DJ01-alkyl** has an absorption maximum peak at 350 nm, and **PR01-alkyl** has a strong absorption maximum peak at 335 nm with a weak shoulder peak at 365 nm, whereas **PM01-alkyl** has an absorption maximum peak at 341 nm. Compared to its counterparts **PR01-alkyl** and **PM01-alkyl**, **DJ01-alkyl** shows a significant bathochromic impact in its UV-vis absorption spectrum. This could be because the thiophene unit enhances the overall conjugation in **DJ01-alkyl** and often leads to a bathochromic shift.[57] The emission maxima (λ_{em}^{max}) of **DJ01-alkyl**, **PR01-alkyl**, and **PM01-alkyl** from the photoluminescence (PL) analysis are 496 nm, 500 nm, and 488 nm, respectively. Additionally, thin-film absorption and emission spectra were recorded, which are displayed in Fig. 2b. It is observed that these molecules in thin films show slightly red shifted spectra in the lower energy absorption band compared to those in solution, indicating that intermolecular π–π interactions exist in these thin

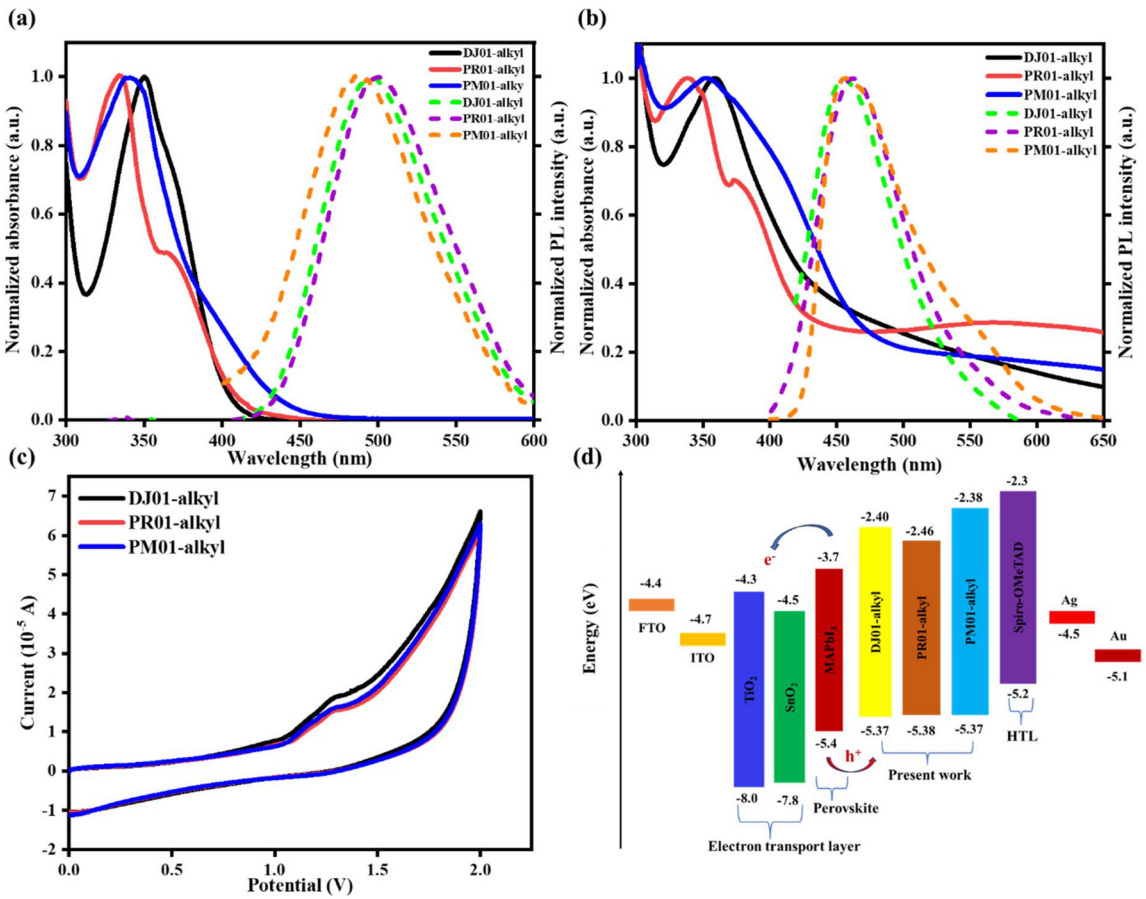

Fig. 2 (a) Normalized UV-vis absorption and fluorescence emission spectra of **DJ01-alkyl**, **PR01-alkyl**, and **PM01-alkyl** in DMSO solution; (b) normalized absorption and emission spectra in thin films; (c) cyclic voltammograms in THF-$TBAPF_6$ (0.1 M), scan speed: 100 mV s^{-1}, potentials *vs.* Fc/Fc^+ and (d) energy level diagram.

Table 1 Optical, thermal, electrochemical and electrical properties of the HTMs

HTMs	λ_{abs} (nm)	λ_{em}^{max} (nm)	λ_{int}^{sol} (nm)	$E_{g\ opt}^{sol}$ (eV)	λ_{abs}^{film} (nm)	λ_{em}^{film} (nm)	λ_{int}^{film} (nm)	T_d (°C)	T_g (°C)	T_m (°C)	HOMO (eV)	LUMO (eV)	μ ($cm^2\ V^{-1}\ s^{-1}$)
DJ01-alkyl	350 (max)	496	418	2.96	359	455	424	357	—	116	−5.37	−2.40	1.7×10^{-5}
PR01-alkyl	335 (max), 365	500	424	2.92	338	462	426	326	—	118	−5.38	−2.46	2.1×10^{-5}
PM01-alkyl	341 (max)	488	415	2.98	352	457	436	314	122	158	−5.37	−2.38	1.6×10^{-5}

films.[50,58,59] Based on the corresponding intersection values of **DJ01-alkyl** (418 nm), **PR01-alkyl** (424 nm), and **PM01-alkyl** (416 nm), the optical band-gap energies were found to be 2.96 eV for **DJ01-alkyl**, 2.92 eV for **PR01-alkyl**, and 2.98 eV for **PM01-alkyl**, respectively. Additionally, Fig. 3 and Fig. S14 display photographs of the synthesised compounds in DMSO solution (1×10^{-5} M) and powders in normal light, short UV light, and long UV light. In addition, quinine sulfate solution in 0.1 N H_2SO_4 was used as a standard to determine the relative fluorescence quantum yields (Φ_f) of the compounds in DMSO. The obtained Φ_f values were 52.90% (**DJ01-alkyl**), 49.05% (**PR01-alkyl**) and 3.50% (**PM01-alkyl**), respectively.

The energy levels of the HTMs were experimentally determined *via* cyclic voltammetry (CV) measurements. The CVs of the HTMs in THF solution are shown in Fig. 2c (Table 1 provides a summary of the data). This figure shows that **DJ01-alkyl**, **PR01-alkyl**, and **PM01-alkyl** all had one oxidation peak. The three compounds showed first oxidation potentials of 1.001, 1.011, and 1.005 eV, respectively. From the onset oxidation (E_{ox}^{onset}), the HOMOs of these compounds were found to be −5.37 eV for **DJ01-alkyl**, −5.38 eV for **PR01-alkyl** and −5.37 eV for **PM01-alkyl**, which were deeper than that of Spiro-OMeTAD (−5.2 eV).[60] The device's higher open-circuit voltage (V_{oc}) may be enhanced by the deeper HOMO levels of the HTMs.[61] The optical band-gap energies were added to the lowest unoccupied molecular orbital (LUMO) energies to determine the HOMO energy level.[62] Furthermore, the LUMO energy levels were calculated to be −2.40 eV, −2.46 eV and −2.38 eV, respectively. Hence, the higher LUMO energy levels may be able to more successfully stop electron transport into the metal electrode.

2.3 Thermal and hydrophobic properties

The thermal properties of these HTMs were investigated using differential scanning calorimetry (DSC) measurements and thermogravimetric analysis (TGA) (Fig. 4a and b). The temperatures of decomposition (T_d or 5% weight loss temperature) for **DJ01-alkyl**, **PR01-alkyl**, and **PM01-alkyl** are approximately 357 °C, 326 °C, and 314 °C, respectively, indicating the molecules' strong thermal stability. Using DSC under nitrogen at a heating rate of 10 °C min^{-1}, the phase transition behaviour of the compound was examined. Although neither the **DJ01-alkyl** nor the **PR01-alkyl** molecules displayed a glass transition temperature (T_g), their respective melting points (T_m) were found to be 116 °C and 118 °C, respectively. However, 122 °C was identified as the T_g and 158 °C as the T_m of **PM01-alkyl**. The conjugation between the nitro group and the phenyl ring restricts the rotational freedom along the main chain, thereby increasing the rigidity of **PM01-alkyl**. Also, the strong polarity of the nitro group assists in the enhancement of intermolecular forces and restriction of molecular mobility, which resulted in the observed T_g.[63] Furthermore, it is evident that the T_g of **PM01-alkyl** is marginally comparable to that of Spiro-OMeTAD (120 °C), which is better for the cell encapsulation process.[64]

As shown in Fig. S15, the water contact angles on **DJ01-alkyl**, **PR01-alkyl**, and **PM01-alkyl** films are found to be 78.9°, 81.2°, and 73.9°, respectively, indicating their hydrophobic nature. Such hydrophobicity enables these HTMs to effectively inhibit moisture penetration into the perovskite layer. In contrast, the dopant free Spiro-OMeTAD-based HTM film exhibits a lower contact angle of 75°, signifying a higher affinity toward

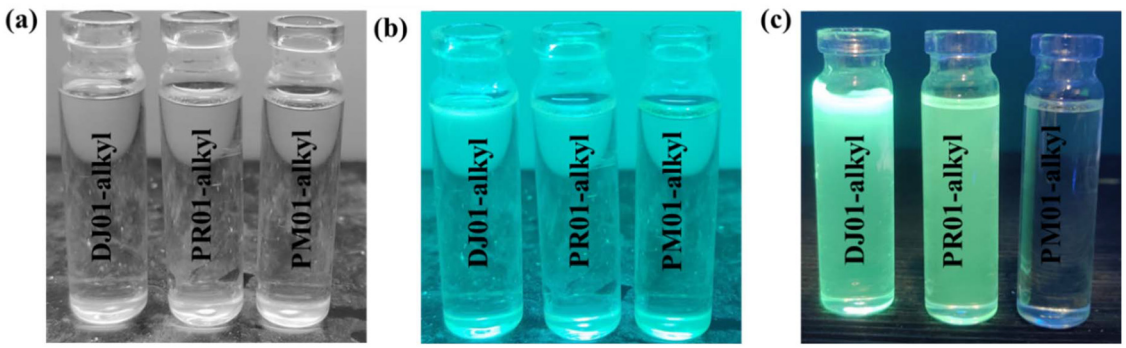

Fig. 3 Photographic images of **DJ01-alkyl**, **PR01-alkyl**, and **PM01-alkyl** in DMSO solution (1×10^{-5} M): (a) normal light; (b) short UV light and (c) long UV light.

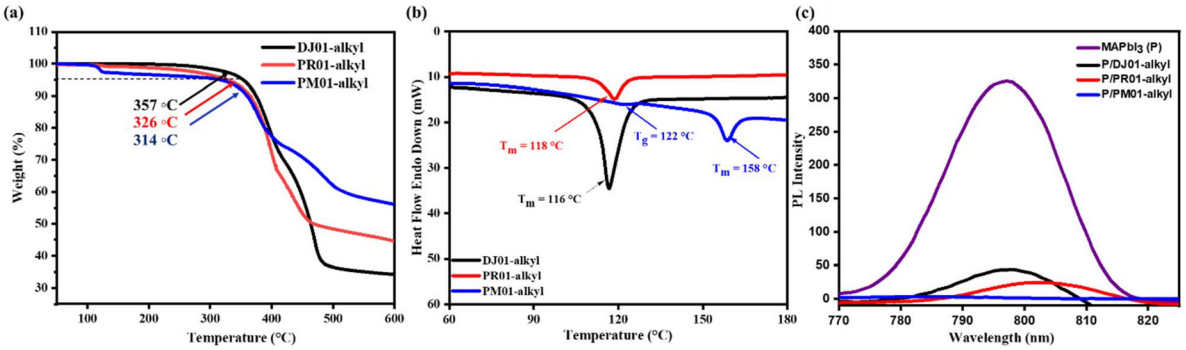

Fig. 4 (a) TGA profiles; (b) DSC profiles and (c) steady state PL spectra of pristine, **DJ01-alkyl**, **PR01-alkyl** and **PM01-alkyl**.

ambient moisture.[65] These results clearly demonstrate that **DJ01-alkyl** and **PR01-alkyl** possess enhanced hydrophobic characteristics compared to Spiro-OMeTAD, thereby providing a more efficient moisture barrier and potentially improving the long-term stability of PSCs. Furthermore, **PR01-alkyl** exhibits the highest water contact angle among the three, suggesting its superior moisture resistance relative to **DJ01-alkyl** and **PM01-alkyl**.

2.4 Steady state photoluminescence

The steady-state photoluminescence (PL) was measured for the synthesized HTMs in order to better understand their hole extraction efficiency. As a reference, the steady-state PL spectrum of the pristine perovskite layer without any HTL was also measured (Fig. 4c). In agreement with the emission peak of $MAPbI_3$, the bare perovskite films exhibited an emission peak at 797 nm. Additionally, a dampening of the PL intensity was seen in all perovskite thin films with HTLs. A more effective hole extraction procedure at the perovskite–HTM interface is shown by the higher PL quenching value of the HTM coated perovskite layer when compared to the bare perovskite layer. These findings show that, in accordance with their hole mobility, **DJ01-alkyl** and **PR01-alkyl** have higher hole extraction efficiency than **PM01-alkyl**.

3. DFT study

3.1 Computational methods

The B3LYP/6-311G(d) level of theory was used to optimize the geometries of all molecules because of its high accuracy in energy and ability to take into account additional parameters, such as atomic orbitals. This basis set was chosen in order to forecast the optical absorption characteristics of the planned HTMs and to optimize the conductor-like polarizable continuum model (CPCM) in DMSO solvent. Frontier molecular orbitals (FMOs) are crucial for understanding and forecasting how charges flow in molecules because they provide information on carrier injection and transportation. The chosen DFT functional was used to compute electron affinity (EA), ionization potential (IP), chemical hardness (η), electrostatic potential (ESP), reorganization energy (RE), transition density matrix (TDM), and density of states (DOS).

3.2 Structural analysis and frontier molecular orbitals

The dihedral angles of the molecules being studied are shown in Fig. 5. They were examined to obtain information about the planarity of the molecules, which is essential for simple charge mobility. On the other hand, all three compounds have about the same dihedral angles between the carbazole and cyanopyridine units. Three segments make up compound **DJ01-alkyl**: carbazole, cyanopyridine, and thiophenyl. The cyanopyridine unit attached to the carbazole is severely distorted out-of-plane, with a dihedral angle of 44.9° on one side and a slight twist of −2.6° with the thiophenyl portion on the other. **PR01-alkyl** has a highly distorted angle between the cyanopyridine and carbazole (44.3°) and the cyanopyridine and 4-bromophenyl (−22.9°) units. Also, **PM01-alkyl** has a highly distorted angle between the cyanopyridine and carbazole (44.2°) and the cyanopyridine and 4-nitrophenyl (−24.3°) units. Among the three synthesized compounds, **DJ01-alkyl** is more planar than **PR01-alkyl** and **PM01-alkyl**.

The frontier molecular orbitals (FMOs) consist of the HOMO and the LUMO. Analysis of the electronic distribution within these orbitals provides valuable insight into the intramolecular charge transfer (ICT) characteristics of a molecule.[66] As shown in Fig. 5, the HOMO is distributed mainly at carbazole units, and the LUMO is located at the core and some part of the end group in the case of **DJ01-alkyl** and **PR01-alkyl**, whereas in the case of **PM01-alkyl** the electron is mainly located at the nitrophenyl group and some part of the core. The computational energy level diagram is shown in Fig. 6d. The synthesized molecules exhibit HOMO energy levels between −5.83 eV and −5.84 eV and LUMO energy levels in the range of −2.31 eV to −3.06 eV. From the present design strategy of D–A–D and A–A–D architectures, it can be inferred that there is no significant alteration in their HOMO energy levels in the case of experimentally and theoretically obtained values.

The available experimental data and the computed maximum absorption wavelengths (λ_{max}^{abs}) of the **DJ01-alkyl**, **PR01-alkyl**, and **PM01-alkyl** HTMs were contrasted (refer to Fig. 6a–c). All things considered, the vertical excitation of

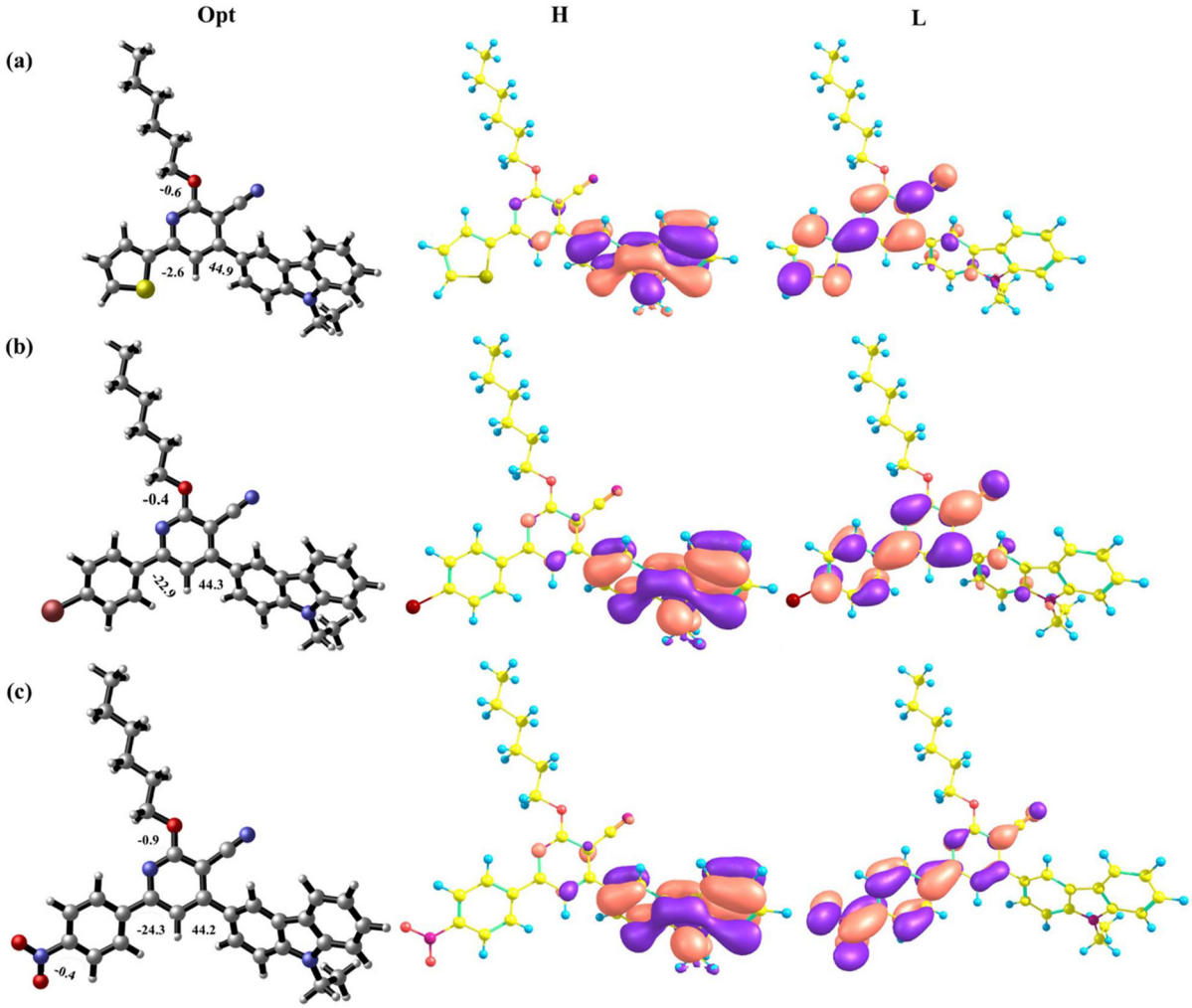

Fig. 5 Optimised structures and frontier molecular orbital contour plots for the studied molecules of (a) **DJ01-alkyl**, (b) **PR01-alkyl**, and (c) **PM01-alkyl**.

these HTMs is better described by the long-range corrected functional approximations of B3LYP, which also show excellent agreement with experimental data. Since B3LYP agrees with the experimental data the best out of the three functional approximations, it is used in this study.

3.3 Reorganization energy, electron affinity, ionization potential and stability

Reorganization energy is a metric used to quantify charge carrier mobilities and approximate charge transfer (CT) characteristics. The excitons must go in the direction of the corresponding electrodes after splitting into electrons and holes in order for them to recombine. The two forms of reorganization energies are external λ_{ext}, which changes with external parameters like the polarization of the surrounding environment, and internal λ_{int}, which depends on the interior geometry of the molecule.[66] According to Marcus theory, this energy's characterisation reveals the transfer rate; a larger charge-transport rate is indicated by a lower k value.[67,68] Table 2 shows that for the reorganization energies, the λ_h values of **DJ01-alkyl**, **PR01-alkyl** and **PM01-alkyl** are 0.10 eV, 0.09 eV and 0.10 eV. It can be observed that these compounds are expected to exhibit excellent hole transport properties.

Also, we calculated the ionization potential (IP) and electron affinity (EA) of the synthesized compounds from their optimized cationic, anionic, and neutral geometries (see Fig. 7). Further, Table 2 shows the IP and EA values that were computed. In comparison with Spiro-OMeTAD (4.47 and 1.07 eV, respectively), the systems under study exhibited comparatively higher IP (5.42–5.65 eV) and EA (2.34–2.75 eV) values,[3] proving the stability of the hole transport materials in terms of the compounds' ability to withstand oxidation. Chemical hardness is a measure of how difficult it is for a molecule to share electrons with the surrounding medium.

$$\eta \cong 1/2\ (\mathrm{IP} - \mathrm{EA}) \quad (1)$$

In this case, electron affinity and ionization potential are reciprocally connected to IP and EA. The more stability a

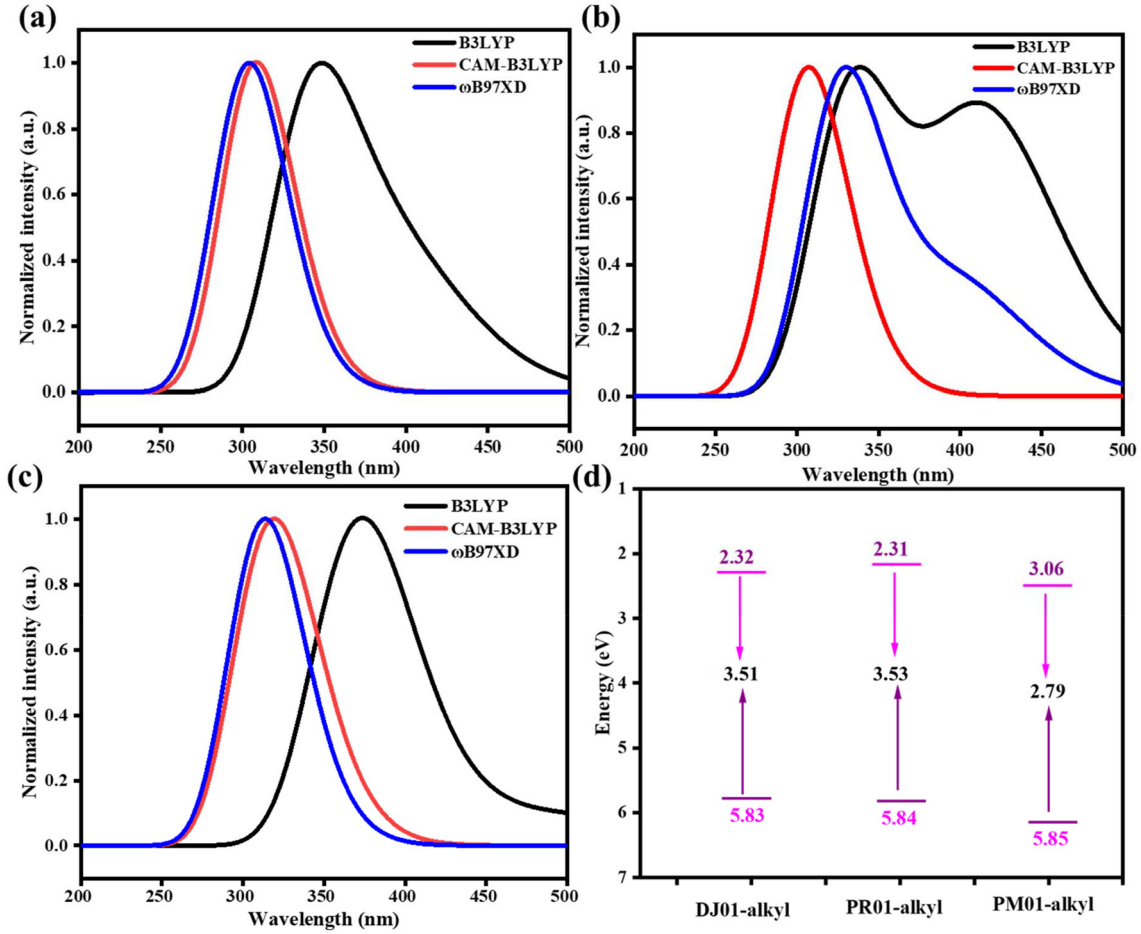

Fig. 6 Absorption data measured in DMSO of (a) **DJ01-alkyl**, (b) **PR01-alkyl**, and (c) **PM01-alkyl** along with their oscillator strength at the TD-DFT/B3LYP/CAM-B3LYP/ωB97XD/CPCM (DMSO) level of theory and (d) band gap plots of the designed molecules plotted using Origin software.

Table 2 Computed optical, electrochemical, reorganization energies and stability values

HTMs	λ_{abs} (nm)	HOMO (eV)	LUMO (eV)	E_g (eV)	IP (eV)	EA (eV)	λ_h (eV)	λ_e (eV)	η (eV)
DJ01-alkyl	350	−5.83	−2.32	3.51	5.63	2.18	0.10	0.435	1.39
PR01-alkyl	335, 365	−5.84	−2.31	3.53	5.63	2.34	0.09	0.367	1.64
PM01-alkyl	341	−5.85	−3.06	2.79	5.65	2.75	0.10	0.70	1.45

system has, the higher its hardness value is. The chemical hardness values are as follows: **DJ01-alkyl** – 1.39 eV, **PR01-alkyl** – 1.64 eV, and **PM01-alkyl** – 1.45 eV. Among the three synthesized compounds **PR01-alkyl** shows a comparable hardness value to spiro-OMeTAD (1.62 eV).

3.4 Electrostatic surface potential (ESP)

The ESP, which characterizes the charge density distribution on a system backbone and is essential for forecasting a molecule's behaviour, is a crucial metric for understanding the stability of molecules.[2] The electrophilic and nucleophilic sites, respectively, are shown by the positive and negative ESP areas, suggesting possible intermolecular interactions.[2] The negative sites are mainly found at the cyano (CN) group due to their electron withdrawing nature in contrast to the positive charge located all over the molecules in the case of **DJ01-alkyl** and **PR01-alkyl** (Fig. 8). On the other hand, the negative charge is also located at the nitro group in the case of **PM01-alkyl**, and it is also believed that the nitro ($-NO_2$) group present in a molecular architecture can interact with Pb^{2+} defect sites of a perovskite, and therefore, it significantly reduces the surface defects of the perovskite, as reported by Subramani *et al.*[69] However, the ESP map of molecules evidently shows that the cyano group is the major negative charge bearing site in all three molecules and the cyano group can interact effectively with the Pb^{2+} of the perovskite and thus passivate the defects.[58]

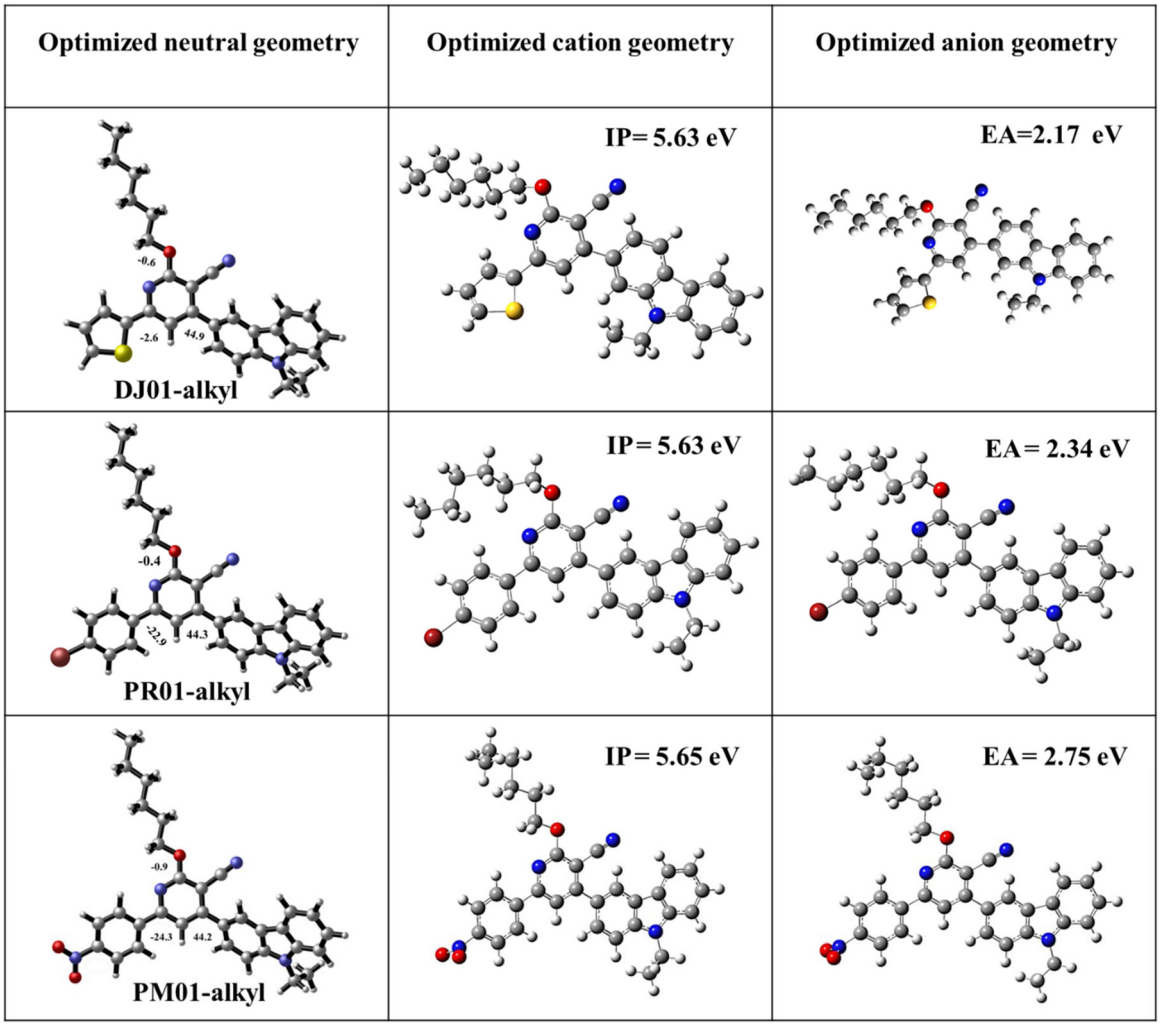

Fig. 7 Schematic representations of the optimized neutral, cationic, and anionic geometries of the synthesized compounds along with their ionization potential (IP) and electron affinity (EA) values.

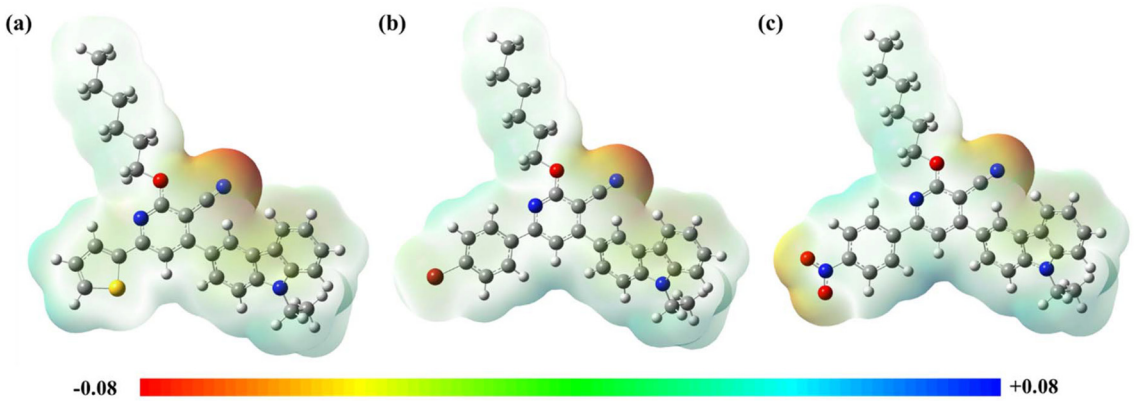

Fig. 8 Electrostatic surface potentials of (a) **DJ01-alkyl**, (b) **PR01-alkyl** and (c) **PM01-alkyl**.

3.5 Transition density matrix and density of states (DOS)

The nature of electrical transitions in a molecule is essentially connected to the features of ICT. Transition density matrix (TDM) analysis was performed for the compounds under investigation in the first excited state (S1), as shown in Fig. 9a–c, in order to assess these kinds of transitions.[70,71] Two prevalent charge transfer types are shown: local excitation (LE) and CT excitation. The excitation mode is LE if the matrix elements are distributed diagonally, whereas CT excitation is the primary excitation mode if the matrix elements are distributed non-diagonally.[70] Hence, we can observe non-diagonal charge transfer in the case of **DJ01-alkyl**, **PR01-alkyl**, and **PM01-alkyl**, which suggests that CT takes place within the molecules. We also performed DOS studies to confirm our analysis of FMOs (Fig. 9d–f). These computations aid in our comprehension of the roles that various chemical orbitals play in electrical processes.[71–73] The *N*-ethylcarbazole groups are shown using the blue band in the plots, while the core (cyanopyridine) and the terminal units are shown using the green and purple bands, whereas hexyloxy is shown using the red colour band, respectively.

The total charge transfer between orbitals is shown using the black band. The donor component, *N*-ethylcarbazole, has a HOMO density in molecules, as can be seen from the picture. The LUMO is mainly composed of cyanopyridine and thiophenyl and 4-bromophenyl for **DJ01-alkyl** and **PR01-alkyl**, whereas, in the case of **PM01-alkyl**, the LUMO is mainly localised in 4-nitrophenyl and some part of the core.

4. Charge mobility

Furthermore, we examined the hole-transporting capabilities of the synthesized compounds by performing xerographic time-of-flight (XTOF) measurements. Table 3 provides the values of the charge mobility defining parameters, zero field mobility (μ_0), and the mobility under an electric field of 1×10^6 V cm^{-1}. Fig. 10a–c shows the field dependence of compounds' hole drift mobility. Among the three compounds, the hole mobility value of **PR01-alkyl** (2.1×10^{-5} cm^2 V^{-1} s^{-1}) is higher than those of **DJ01-alkyl** (1.7×10^{-5} cm^2 V^{-1} s^{-1}) and **PM01-alkyl** (1.6×10^{-5} cm^2 V^{-1} s^{-1}), which also corresponds to the theoretically obtained trends of hole transporting rates.

In all the cases investigated, the mobility μ is approximated using the formula

$$\mu = \mu_0 \exp(\beta\sqrt{E}),$$

where μ_0 is the zero field mobility, β is the field dependence parameter, and E is the electric field strength. The values of mobility defining parameters μ_0 and β as well as the mobility value at the 1×10^6 V cm^{-1} field strength are obtained from the fitting data shown in Fig. 10d–f. Hole transport in these materials is characterized by high values of coefficient β and this is a consequence of high transport dispersion. This also indicates a high disorder of the energetic distribution of hole transport states.[74] Joseph *et al.*[75] synthesized four HTMs, whose μ values were calculated using the XTOF technique: **DImP-4D** – ~6×10^{-5} cm^2 V^{-1} s^{-1}, **DImF-4D** – 8.8×10^{-5} cm^2

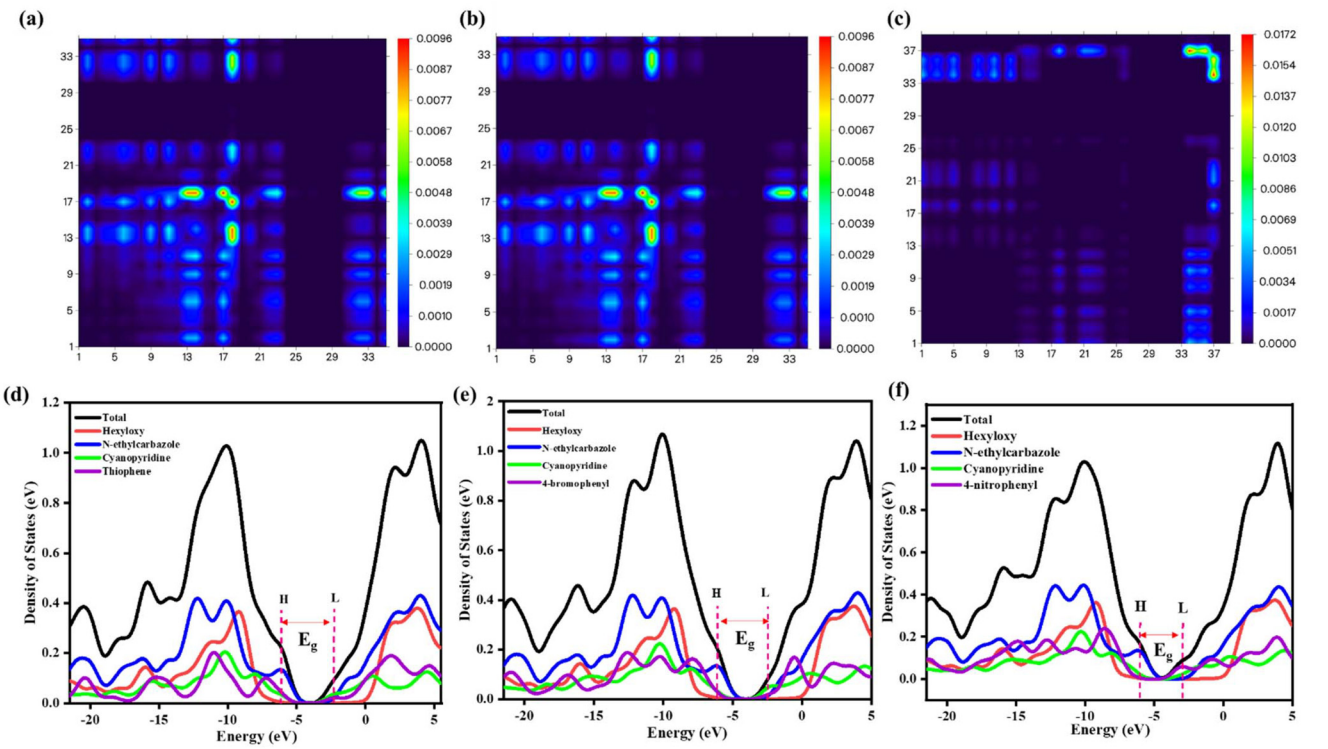

Fig. 9 Transition density matrixes of (a) **DJ01-alkyl**, (b) **PR01-alkyl**, and (c) **PM01-alkyl**; and densities of states (DOS) of (d) **DJ01-alkyl**, (e) **PR01-alkyl** and (f) **PM01-alkyl**.

Table 3 Hole mobility values for **DJ01-alkyl**, **PR01-alkyl**, **PM01-alkyl**, Spiro-OMeTAD and some reported HTMs

HTMs	μ_0 ($cm^2\ V^{-1}\ s^{-1}$)	β ($(cm\ V^{-1})^{0.5}$)	μ ($cm^2\ V^{-1}\ s^{-1}$)	Ref.
DJ01-alkyl	8×10^{-9}	~0.0077	1.7×10^{-5}	Present work
PR01-alkyl	6×10^{-9}	0.0083	2.1×10^{-5}	Present work
PM01-alkyl	5×10^{-9}	0.0081	1.6×10^{-5}	Present work
Spiro-OMeTAD	1×10^{-4}	—	2.1×10^{-3}	76
DJ01	1.5×10^{-7}	0.0049	1.7×10^{-5}	50
PR01	$\sim 1 \times 10^{-9}$	0.0093	1.2×10^{-5}	50
DImP-4D	—	—	$\sim 6 \times 10^{-6}$	75
DImF-4D	1.2×10^{-7}	0.0054	8.8×10^{-6}	75
DImT-4D	—	—	$\sim 2 \times 10^{-6}$	75
DImBT-4D	$\sim 5 \times 10^{-8}$	~0.0059	5.5×10^{-6}	75
HD1	7.50×10^{-7}	0.0072	1×10^{-5}	77
HD2	5.27×10^{-7}	0.0050	4.4×10^{-5}	77
HD3	1.91×10^{-6}	0.0029	1.1×10^{-3}	77
HD4	—	—	6.1×10^{-4}	77

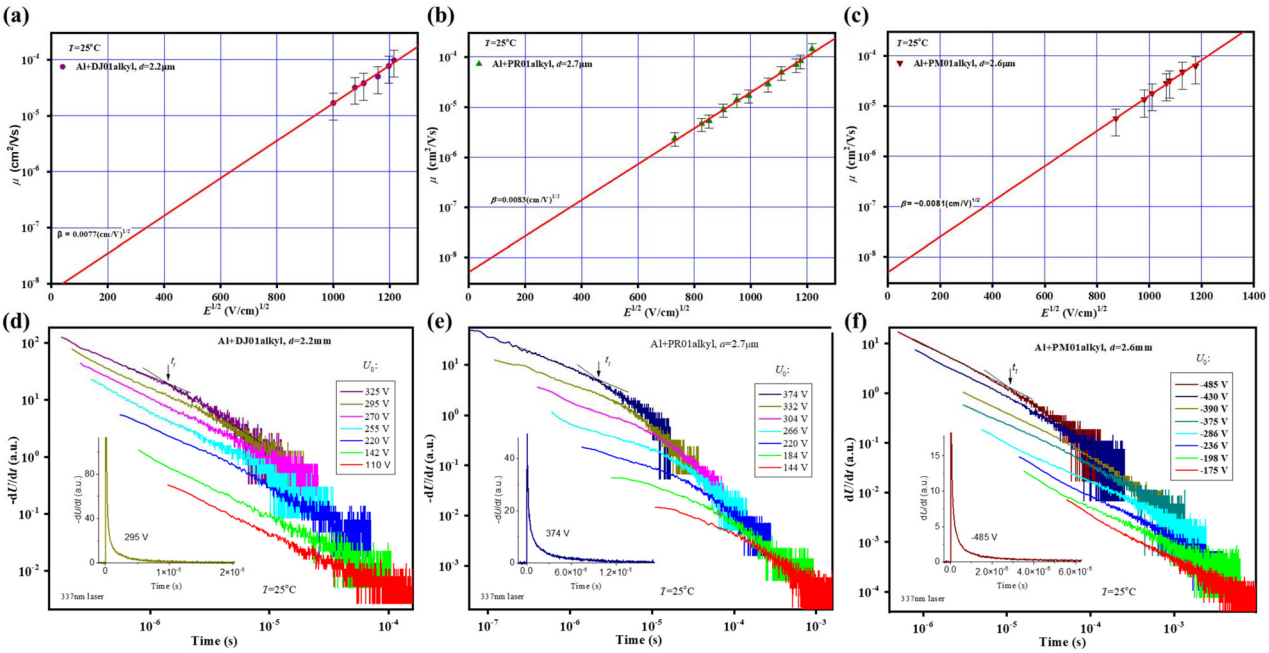

Fig. 10 Field dependence of hole drift mobility for (a) **DJ01-alkyl**, (b) **PR01-alkyl**, and (c) **PM01-alkyl**; and transient photocurrents in the layers of (d) **DJ01-alkyl**, (e) **PR01-alkyl** and (f) **PM01-alkyl** at different sample voltages.

$V^{-1}\ s^{-1}$, **DImT-4D** – $\sim 2 \times 10^{-5}$ $cm^2\ V^{-1}\ s^{-1}$ and **DImBT-4D** – $\sim 5.5 \times 10^{-5}$ $cm^2\ V^{-1}\ s^{-1}$. Among the four molecules, **DImBT-4D** achieved the best PCE of 20.11%. Furthermore, when compared with our previously synthesized molecules DJ01 (1.7×10^{-5} $cm^2\ V^{-1}\ s^{-1}$) and PR01 (1.2×10^{-5} $cm^2\ V^{-1}\ s^{-1}$), the newly synthesized molecules exhibit improved hole mobility, primarily due to their enhanced solubility, which facilitates the formation of uniform thin films and efficient charge transport. In contrast, the hole mobility of PM01 could not be reliably measured because of its poor and complex solubility and film-forming behavior, whereas **PM01-alkyl** showed measurable hole mobility, owing to alkylation-induced improvement in solubility and film quality. These reports support and further suggest that our three synthesized molecules can also serve as effective HTMs for the fabrication of PSCs. Furthermore, Table 3 shows that our molecules are better in terms of hole mobility when compared to other HTMs.

5. Conclusion

In summary, three new HTMs, **DJ01-alkyl**, **PR01-alkyl**, and **PM01-alkyl**, were successfully designed and synthesised. Their charge-transporting, photophysical, thermal, and electrochemical properties were systematically examined. All the molecules exhibited good thermal stabilities. Furthermore, the compounds possessed higher LUMO energy levels in the range

of −2.38 eV to −2.46 eV and deeper HOMO energy levels in the range of −5.37–5.38 eV. Additionally, these compounds demonstrated improved solubility in widely used organic solvents. Additionally, DFT calculations were conducted to correlate the experimentally observed results. Among the three compounds, **PR01-alkyl** (2.1×10^{-5} cm^2 V^{-1} s^{-1}) exhibited greater hole mobility than **DJ01-alkyl** (1.7×10^{-5} cm^2 V^{-1} s^{-1}) and **PM01-alkyl** (1.6×10^{-5} cm^2 V^{-1} s^{-1}), and these molecular trends coincide well with the molecular trends observed for the reorganization energy that were theoretically obtained. Finally, due to the low cost, these materials show a lot of potential for application as affordable, effective hole transport substances and might be suitable substitutes for the expensive Spiro-OMeTAD.

Conflicts of interest

There are no conflicts to declare.

Data availability

The data supporting this article have been included as part of the supplementary information (SI). The supporting information file contains the synthesis procedure, cost calculation, crystal data, ATR-IR, NMR, Mass spectra, photographic images, contact angle cyclic voltamograms, computational details, *etc*. See DOI: **https://doi.org/10.1039/d6qo00076b**.

CCDC 2500277 and 2455342 contain the supplementary crystallographic data for this paper.[78a,b]

Acknowledgements

Ahipa is thankful to JAIN (Deemed-to-be University), Bengaluru (Bangalore), Karnataka, India, for support under a Minor Project Grant (Ref. No.: JU/MRP/CNMS/101/2025) and the Science and Engineering Research Board (SERB), Govt. of India, New Delhi, India, for support under a Core Research Grant (Project File No.: CRG/2020/003151). Arijit is grateful to JAIN (Deemed-to-be University), Bangalore, Karnataka, India for a Postdoctoral Fellowship (Ref. No.: JU/APP/CNMS/2025/552). K. R. and V. G. received funding from the Research Council of Lithuania (LMTLT), Agreement No. S-AUEI-23-1 (22-12-2023).

References

1 K. Rakstys, C. Igci and M. K. Nazeeruddin, Efficiency vs. stability: dopant-free hole transporting materials towards stabilized perovskite solar cells, *Chem. Sci.*, 2019, **10**(28), 6748–6769.

2 Z. Wang, C. Xu, Z. Yang, Y. Zou, K. Zhang, P. Gao, W. Xu, G. Li, J. Chen and M. Liang, Dithieno[3,2-a:2′,3′-c]phenazine based hole-transporting materials for efficient perovskite solar cells: Effects of donors numbers, *Dyes Pigm.*, 2023, **211**, 111066.

3 A. Idrissi, Z. El Fakir, R. Atir, A. Habsaoui, M. E. Touhami and S. Bouzakraoui, Thiophene-based molecules as hole transport materials for efficient perovskite solar cells or as donors for organic solar cells, *Mater. Chem. Phys.*, 2023, **293**, 126851.

4 A. Kojima, K. Teshima, Y. Shirai and T. Miyasaka, Organometal Halide Perovskites as Visible-Light Sensitizers for Photovoltaic Cells, *J. Am. Chem. Soc.*, 2009, **131**(17), 6050–6051.

5 H. Zhang, K. Darabi, N. Y. Nia, A. Krishna, P. Ahlawat, B. Guo, M. H. S. Almalki, T.-S. Su, D. Ren, V. Bolnykh, L. A. Castriotta, M. Zendehdel, L. Pan, S. S. Alonso, R. Li, S. M. Zakeeruddin, A. Hagfeldt, U. Rothlisberger, A. Di Carlo, A. Amassian and M. Grätzel, A universal co-solvent dilution strategy enables facile and cost-effective fabrication of perovskite photovoltaics, *Nat. Commun.*, 2022, **13**(1), 89.

6 M. A. Truong, H. Lee, A. Shimazaki, R. Mishima, M. Hino, K. Yamamoto, K. Otsuka, T. Handa, Y. Kanemitsu, R. Murdey and A. Wakamiya, Near-Ultraviolet Transparent Organic Hole-Transporting Materials Containing Partially Oxygen-Bridged Triphenylamine Skeletons for Efficient Perovskite Solar Cells, *ACS Appl. Energy Mater.*, 2021, **4**(2), 1484–1495.

7 Q. Tai, K.-C. Tang and F. Yan, Recent progress of inorganic perovskite solar cells, *Energy Environ. Sci.*, 2019, **12**(8), 2375–2405.

8 K.-M. Lee, S. Y. Abate, J. H. Yang, W.-H. Chiu, S. Ahn, S.-R. Li, K.-L. Liau, Y.-T. Tao and Y.-D. Lin, Facile synthesis of spiro-core-based hole-transporting material for high-performance and stable perovskite solar cells, *Chem. Eng. J.*, 2023, **454**, 139926.

9 H. Wang, A. D. Sheikh, Q. Feng, F. Li, Y. Chen, W. Yu, E. Alarousu, C. Ma, M. A. Haque, D. Shi, Z.-S. Wang, O. F. Mohammed, O. M. Bakr and T. Wu, Facile Synthesis and High Performance of a New Carbazole-Based Hole-Transporting Material for Hybrid Perovskite Solar Cells, *ACS Photonics*, 2015, **2**(7), 849–855.

10 R. Grisorio, R. Iacobellis, A. Listorti, L. De Marco, M. P. Cipolla, M. Manca, A. Rizzo, A. Abate, G. Gigli and G. P. Suranna, Rational Design of Molecular Hole-Transporting Materials for Perovskite Solar Cells: Direct versus Inverted Device Configurations, *ACS Appl. Mater. Interfaces*, 2017, **9**(29), 24778–24787.

11 Q. Yan, Y. Guo, A. Ichimura, H. Tsuji and E. Nakamura, Three-Dimensionally Homoconjugated Carbon-Bridged Oligophenylenevinylene for Perovskite Solar Cells, *J. Am. Chem. Soc.*, 2016, **138**(34), 10897–10904.

12 N. Onozawa-Komatsuzaki, D. Tsuchiya, S. Inoue, A. Kogo, T. Funaki, M. Chikamatsu, T. Ueno and T. N. Murakami, Highly Efficient Dopant-Free Cyano-Substituted Spiro-Type Hole-Transporting Materials for Perovskite Solar Cells, *ACS Appl. Energy Mater.*, 2022, **5**(6), 6633–6641.

13 T. Bie, R. Li, X. Gao, L. Yang, P. Ma, D. Zhang, Y. Xue, J. Wen, Z. Wang, X. Ma and M. Shao, Halogen-

Functionalized Hole Transport Materials with Strong Passivation Effects for Stable and Highly Efficient Quasi-2D Perovskite Solar Cells, *ACS Nano*, 2024, **18**(34), 23615–23624.

14 A. K. Jena, Y. Numata, M. Ikegami and T. Miyasaka, Role of spiro-OMeTAD in performance deterioration of perovskite solar cells at high temperature and reuse of the perovskite films to avoid Pb-waste, *J. Mater. Chem. A*, 2018, **6**(5), 2219–2230.

15 M.-C. Jung, S. R. Raga, L. K. Ono and Y. Qi, Substantial improvement of perovskite solar cells stability by pinhole-free hole transport layer with doping engineering, *Sci. Rep.*, 2015, **5**(1), 9863.

16 Y. Feng, Q. Hu, E. Rezaee, M. Li, Z.-X. Xu, A. Lorenzoni, F. Mercuri and M. Muccini, High-Performance and Stable Perovskite Solar Cells Based on Dopant-Free Arylamine-Substituted Copper(II) Phthalocyanine Hole-Transporting Materials, *Adv. Energy Mater.*, 2019, **9**(26), 1901019.

17 Y. Feng, Q. Chen, L. Dong, Z. Zhang, C. Li, S. Yang, S. Cai and Z.-X. Xu, Carbon-chain length substituent effects on Cu(II) phthalocyanines as dopant-free hole-transport materials for perovskite solar cells, *Sol. Energy*, 2019, **184**, 649–656.

18 C. Liu, C. Igci, Y. Yang, O. A. Syzgantseva, M. A. Syzgantseva, K. Rakstys, H. Kanda, N. Shibayama, B. Ding, X. Zhang, V. Jankauskas, Y. Ding, S. Dai, P. J. Dyson and M. K. Nazeeruddin, Dopant-Free Hole Transport Materials Afford Efficient and Stable Inorganic Perovskite Solar Cells and Modules, *Angew. Chem., Int. Ed.*, 2021, **60**(37), 20489–20497.

19 K. Rakstys, S. Paek, P. Gao, P. Gratia, T. Marszalek, G. Grancini, K. T. Cho, K. Genevicius, V. Jankauskas, W. Pisula and M. K. Nazeeruddin, Molecular engineering of face-on oriented dopant-free hole transporting material for perovskite solar cells with 19% PCE, *J. Mater. Chem. A*, 2017, **5**(17), 7811–7815.

20 J. Su, X. Zhang, Z. Dong, H. Pan, F. Zhang, X. Li, S. Wang and Z. Chen, Efficient Perovskite Solar Cells by Employing Triphenylamine-Functionalized Azadipyrromethene Dyes as Dopant-Free Hole-Transporting Materials and Bidentate Surface Passivating Agents, *ACS Appl. Mater. Interfaces*, 2024, **16**(38), 51241–51252.

21 D. Zhang, P. Xu, T. Wu, Y. Ou, X. Yang, A. Sun, B. Cui, H. Sun and Y. Hua, Cyclopenta[hi]aceanthrylene-based dopant-free hole-transport material for organic–inorganic hybrid and all-inorganic perovskite solar cells, *J. Mater. Chem. A*, 2019, **7**(10), 5221–5226.

22 H. Zhang, H. Wang, W. Chen and A. K.-Y. Jen, CuGaO2: A promising inorganic hole–transporting material for highly efficient and stable perovskite solar cells, *Adv. Mater.*, 2017, **29**(8), 1604984.

23 A. A. Sutanto, V. Joseph, C. Igci, O. A. Syzgantseva, M. A. Syzgantseva, V. Jankauskas, K. Rakstys, V. I. E. Queloz, P.-Y. Huang, J.-S. Ni, S. Kinge, A. M. Asiri, M.-C. Chen and M. K. Nazeeruddin, Isomeric Carbazole-Based Hole-Transporting Materials: Role of the Linkage Position on the Photovoltaic Performance of Perovskite Solar Cells, *Chem. Mater.*, 2021, **33**(9), 3286–3296.

24 H.-S. Kim, C.-R. Lee, J.-H. Im, K.-B. Lee, T. Moehl, A. Marchioro, S.-J. Moon, R. Humphry-Baker, J.-H. Yum, J. E. Moser, M. Grätzel and N.-G. Park, Lead Iodide Perovskite Sensitized All-Solid-State Submicron Thin Film Mesoscopic Solar Cell with Efficiency Exceeding 9%, *Sci. Rep.*, 2012, **2**(1), 591.

25 G.-W. Kim, H. Choi, M. Kim, J. Lee, S. Y. Son and T. Park, Hole Transport Materials in Conventional Structural (n–i–p) Perovskite Solar Cells: From Past to the Future, *Adv. Energy Mater.*, 2020, **10**(8), 1903403.

26 W. Ke, P. Priyanka, S. Vegiraju, C. C. Stoumpos, I. Spanopoulos, C. M. M. Soe, T. J. Marks, M.-C. Chen and M. G. Kanatzidis, Dopant-Free Tetrakis-Triphenylamine Hole Transporting Material for Efficient Tin-Based Perovskite Solar Cells, *J. Am. Chem. Soc.*, 2018, **140**(1), 388–393.

27 W. Rehman, R. L. Milot, G. E. Eperon, C. Wehrenfennig, J. L. Boland, H. J. Snaith, M. B. Johnston and L. M. Herz, Charge-Carrier Dynamics and Mobilities in Formamidinium Lead Mixed-Halide Perovskites, *Adv. Mater.*, 2015, **27**(48), 7938–7944.

28 M. Daskeviciene, S. Paek, Z. Wang, T. Malinauskas, G. Jokubauskaite, K. Rakstys, K. T. Cho, A. Magomedov, V. Jankauskas, S. Ahmad, H. J. Snaith, V. Getautis and M. K. Nazeeruddin, Carbazole-based enamine: Low-cost and efficient hole transporting material for perovskite solar cells, *Nano Energy*, 2017, **32**, 551–557.

29 S. D. Sung, M. S. Kang, I. T. Choi, H. M. Kim, H. Kim, M. Hong, H. K. Kim and W. I. Lee, 14.8% perovskite solar cells employing carbazole derivatives as hole transporting materials, *Chem. Commun.*, 2014, **50**(91), 14161–14163.

30 B. Xu, E. Sheibani, P. Liu, J. Zhang, H. Tian, N. Vlachopoulos, G. Boschloo, L. Kloo, A. Hagfeldt and L. Sun, Carbazole-Based Hole-Transport Materials for Efficient Solid-State Dye-Sensitized Solar Cells and Perovskite Solar Cells, *Adv. Mater.*, 2014, **26**(38), 6629–6634.

31 O. Ostroverkhova, Organic Optoelectronic Materials: Mechanisms and Applications, *Chem. Rev.*, 2016, **116**(22), 13279–13412.

32 S. Ma, X. Zhang, X. Liu, R. Ghadari, M. Cai, Y. Ding, M. Mateen and S. Dai, Pyridine-triphenylamine hole transport material for inverted perovskite solar cells, *J. Energy Chem.*, 2021, **54**, 395–402.

33 P. Huang, Manju, S. Kazim, G. Sivakumar, M. Salado, R. Misra and S. Ahmad, Pyridine Bridging Diphenylamine-Carbazole with Linking Topology as Rational Hole Transporter for Perovskite Solar Cells Fabrication, *ACS Appl. Mater. Interfaces*, 2020, **12**(20), 22881–22890.

34 X. Liu, S. Ma, Y. Ding, J. Gao, X. Liu, J. Yao and S. Dai, Molecular Engineering of Simple Carbazole-Triphenylamine Hole Transporting Materials by Replacing Benzene with Pyridine Unit for Perovskite Solar Cells, *Sol. RRL*, 2019, **3**(5), 1800337.

35 B. Xu, Z. Zhu, J. Zhang, H. Liu, C.-C. Chueh, X. Li and A. K. Y. Jen, 4-Tert-butylpyridine Free Organic Hole

Transporting Materials for Stable and Efficient Planar Perovskite Solar Cells, *Adv. Energy Mater.*, 2017, **7**(19), 1700683.

36 S. S. Reddy, V. M. Arivunithi, V. G. Sree, H. Kwon, J. Park, Y.-C. Kang, H. Zhu, Y.-Y. Noh and S.-H. Jin, Lewis acid-base adduct-type organic hole transport material for high performance and air-stable perovskite solar cells, *Nano Energy*, 2019, **58**, 284–292.

37 L. Duan, Y. Chen, J. Yuan, X. Zong, Z. Sun, Q. Wu and S. Xue, Dopant-free X-shaped D-A type hole-transporting materials for p-i-n perovskite solar cells, *Dyes Pigm.*, 2020, **178**, 108334.

38 I. F. Perepichka and D. F. Perepichka, *Handbook of Thiophene-Based Materials: Applications in Organic Electronics and Photonics*, John Wiley & Sons, 2009, vol. 2.

39 Z.-U.-Rehman, A. Saeed and M. Faisal, Synthesis and characterization of thiophene-mediated hole transport materials for perovskite solar cells, *Synth. Met.*, 2018, **241**, 54–68.

40 A. Krishna and A. C. Grimsdale, Hole transporting materials for mesoscopic perovskite solar cells – towards a rational design?, *J. Mater. Chem. A*, 2017, **5**(32), 16446–16466.

41 E. Rezaee, X. Liu, Q. Hu, L. Dong, Q. Chen, J.-H. Pan and Z.-X. Xu, Dopant-Free Hole Transporting Materials for Perovskite Solar Cells, *Sol. RRL*, 2018, **2**(11), 1800200.

42 S. Ameen, M. S. Akhtar, M. Nazim, M. K. Nazeeruddin and H.-S. Shin, Stable perovskite solar cells using thiazolo [5,4-d]thiazole-core containing hole transporting material, *Nano Energy*, 2018, **49**, 372–379.

43 Z. Gong, R. Wang, Y. Jiang, X. Kong, Y. Lin, Z. Xu, G. Zhou, J.-M. Liu, K. Kempa and J. Gao, Novel D-A-D type small-molecular hole transport materials for stable inverted perovskite solar cells, *Org. Electron.*, 2021, **92**, 106102.

44 H. Xiong, G. DeLuca, Y. Rui, B. Zhang, Y. Li, Q. Zhang, H. Wang and E. Reichmanis, Modifying Perovskite Films with Polyvinylpyrrolidone for Ambient-Air-Stable Highly Bendable Solar Cells, *ACS Appl. Mater. Interfaces*, 2018, **10**(41), 35385–35394.

45 Y. Wang, W. Chen, L. Wang, B. Tu, T. Chen, B. Liu, K. Yang, C. W. Koh, X. Zhang, H. Sun, G. Chen, X. Feng, H. Y. Woo, A. B. Djurišić, Z. He and X. Guo, Dopant-Free Small-Molecule Hole-Transporting Material for Inverted Perovskite Solar Cells with Efficiency Exceeding 21%, *Adv. Mater.*, 2019, **31**(35), 1902781.

46 P.-Y. Su, Y.-F. Chen, J.-M. Liu, L.-M. Xiao, D.-B. Kuang, M. Mayor and C.-Y. Su, Hydrophobic Hole-Transporting Materials Incorporating Multiple Thiophene Cores with Long Alkyl Chains for Efficient Perovskite Solar Cells, *Electrochim. Acta*, 2016, **209**, 529–540.

47 J. Zhang, B. Xu, M. B. Johansson, M. Hadadian, J. P. C. Baena, P. Liu, Y. Hua, N. Vlachopoulos, E. M. J. Johansson, G. Boschloo, L. Sun and A. Hagfeld, Constructive effects of alkyl chains: a strategy to design simple and non-spiro hole transporting materials for high-efficiency mixed-ion perovskite solar cells, *J. Adv. Energy Mater*, 2016, **6**(13), 1502536.

48 C.-H. Chang, R. Griniene, Y.-D. Su, C.-C. Yeh, H.-C. Kao, J. V. Grazulevicius, D. Volyniuk and S. Grigalevicius, Efficient red phosphorescent OLEDs employing carbazole-based materials as the emitting host, *Dyes Pigm.*, 2015, **122**, 257–263.

49 C.-H. Chang, G. Krucaite, D. Lo, Y.-L. Chen, C.-C. Su, T.-C. Lin, J. V. Grazulevicius, L. Peciulyte and S. Grigalevicius, Naphthyl or pyrenyl substituted 2-phenyl-carbazoles as hole transporting materials for organic light-emitting diodes, *Dyes Pigm.*, 2017, **136**, 302–311.

50 R. Chetri, D. Devadiga, K. Rakstys, V. Jankauskas, V. Getautis, R. Ghadari, M. K. Nazeeruddin and A. T. Nagaraja, D–A–D- and A–A–D-Type Cyanopyridone Derivatives as a New Class of Hole-Transporting Materials for Perovskite Solar Cells, *Energy Fuels*, 2025, **39**(1), 852–867.

51 R. Chetri and A. T. Nagaraja, Minireview and Outlook of Carbazole and Phenothiazine-Modified Triphenylamines as Hole Transporting Materials for Enhancing Perovskite Solar Cells, *Energy Fuels*, 2025, **39**(20), 9232–9261.

52 H. A. Sabek, A. M. Alazaly, D. Salah, H. S. Abdel-Samad, M. A. Ismail and A. A. Abdel-Shafi, Photophysical properties and fluorosolvatochromism of D–π–A thiophene based derivatives, *RSC Adv.*, 2020, **10**(71), 43459–43471.

53 Y. Hara, K. Kozuka, K. Imato, S. Akiyama, M. Ishida and Y. Ooyama, Synthesis, and optical and electrochemical properties of 1, 1′, 3, 3′-tetraaryl-4, 4′-bibenzo [c] thiophene derivatives with the same or different aryl substituents on the thiophene rings, *New J. Chem.*, 2024, **48**(22), 9890–9898.

54 C. Janiak, A critical account on π–π stacking in metal complexes with aromatic nitrogen-containing ligands, *J. Chem. Soc., Dalton Trans.*, 2000, (21), 3885–3896.

55 M. Tepliakova, I. K. Yakushenko, E. I. Romadina, A. V. Novikov, P. M. Kuznetsov, K. J. Stevenson and P. A. Troshin, Strength of attraction: pyrene-based hole-transport materials with effective π–π stacking for dopant-free perovskite solar cells, *Sustainable Energy Fuels*, 2021, **5**(1), 283–288.

56 S. P. Thomas, P. R. Spackman, D. Jayatilaka and M. A. Spackman, Accurate Lattice Energies for Molecular Crystals from Experimental Crystal Structures, *J. Chem. Theory Comput.*, 2018, **14**(3), 1614–1623.

57 H. Meier, J. Gerold, H. Kolshorn and B. Mühling, Extension of Conjugation Leading to Bathochromic or Hypsochromic Effects in OPV Series, *Chem. – Eur. J.*, 2004, **10**(2), 360–370.

58 Z. Zhou, X. Zhang, R. Ghadari, X. Liu, W. Wang, Y. Ding, M. Cai, J. H. Pan and S. Dai, CN-based carbazole-arylamine hole transporting materials for perovskite solar cells: Substitution position matters, *J. Energy Chem.*, 2021, **62**, 563–571.

59 J. Mei, Y. Hong, J. W. Y. Lam, A. Qin, Y. Tang and B. Z. Tang, Aggregation-Induced Emission: The Whole Is More Brilliant than the Parts, *Adv. Mater.*, 2014, **26**(31), 5429–5479.

60 M. S. G. Hamed and G. T. Mola, Mixed Halide Perovskite Solar Cells: Progress and Challenges, *Crit. Rev. Solid State Mater. Sci.*, 2020, **45**(2), 85–112.
61 S. Ryu, J. H. Noh, N. J. Jeon, Y. C. Kim, W. S. Yang, J. Seo and S. I. Seok, Voltage output of efficient perovskite solar cells with high open-circuit voltage and fill factor, *Energy Environ. Sci.*, 2014, **7**(8), 2614–2618.
62 J. Wu, C. Liu, B. Li, F. Gu, L. Zhang, M. Hu, X. Deng, Y. Qiao, Y. Mao, W. Tan, Y. Tian and B. Xu, Side-Chain Polymers as Dopant-Free Hole-Transporting Materials for Perovskite Solar Cells—The Impact of Substituents' Positions in Carbazole on Device Performance, *ACS Appl. Mater. Interfaces*, 2019, **11**(30), 26928–26937.
63 X. Tang, C. Din, S. Yu, Y. Liu, H. Luo, D. Zhang and S. Chen, Synthesis of dielectric polystyrene via one-step nitration reaction for large-scale energy storage, *Chem. Eng. J.*, 2022, **446**, 137281.
64 U. Bach, D. Lupo, P. Comte, J. E. Moser, F. Weissörtel, J. Salbeck, H. Spreitzer and M. Grätzel, Solid-state dye-sensitized mesoporous TiO2 solar cells with high photon-to-electron conversion efficiencies, *Nature*, 1998, **395**(6702), 583–585.
65 Y. Hua, S. Chen, D. Zhang, P. Xu, A. Sun, Y. Ou, T. Wu, H. Sun, B. Cui and X. Zhu, Bis[di(4-methoxyphenyl)amino] carbazole-capped indacenodithiophenes as hole transport materials for highly efficient perovskite solar cells: the pronounced positioning effect of a donor group on the cell performance, *J. Mater. Chem. A*, 2019, **7**(17), 10200–10205.
66 U. Azeem, R. A. Khera, A. Naveed, M. Imran, M. A. Assiri, M. Khalid and J. Iqbal, Tuning of a A–A–D–A–A-Type Small Molecule with Benzodithiophene as a Central Core with Efficient Photovoltaic Properties for Organic Solar Cells, *ACS Omega*, 2021, **6**(43), 28923–28935.
67 Z. El Fakir, A. Idrissi, R. Atir and S. Bouzakraoui, Theoretical investigation of DMPA-containing carbazole-based hole-transport materials for perovskite solar cells, *J. Mol. Struct.*, 2024, **1316**, 139059.
68 Z. El Fakir, A. Idrissi, A. Habsaoui and S. Bouzakraoui, Small carbazole-based molecules as hole transporting materials for perovskite solar cells, *J. Mol. Graphics Modell.*, 2023, **122**, 108504.
69 S. Subramani and G. Rajamanickam, 4-Nitrophthalic Acid as an Additive for Low-Cost, Stable, and Efficient Carbon-Based Perovskite Solar Cells, *Langmuir*, 2025, **41**(30), 20420–20431.
70 A. R. Ayub, G. Basharat, S. Arshad, S. Nazir, H. Hamid, S. M. Arshed, M. N. Zahid, J. Iqbal and K. Ayub, A quantum mechanical investigation of nanocone oxide as a drug carrier for zidovudine: AIDS drug, *J. Mol. Graphics Modell.*, 2023, **125**, 108611.
71 M. D. Mohammadi and H. Y. Abdullah, The adsorption of bromochlorodifluoromethane on pristine, Al, Ga, P, and As-doped boron nitride nanotubes: A study involving PBC-DFT, NBO analysis, and QTAIM, *Comput. Theor. Chem.*, 2021, **1193**, 113047.
72 M. U. Khan, J. Iqbal, M. Khalid, R. Hussain, A. A. C. Braga, M. Hussain and S. J. R. Muhammad, Designing triazatruxene-based donor materials with promising photovoltaic parameters for organic solar cells, *RSC Adv.*, 2019, **9**(45), 26402–26418.
73 G. Sivakumar, M. Paramasivam, D. Bharath and V. J. Rao, Energy level tuning of 'Z'-shaped small molecular non-fullerene electron acceptors based on a dipyrrolo[2,3-b:2′,3′-e] pyrazine-2,6(1H,5H)-dione acceptor unit for organic photovoltaic applications: a joint experimental and DFT investigation on the effect of fluorination, *New J. Chem.*, 2019, **43**(13), 5173–5186.
74 H. Bässler, Charge transport in disordered organic photoconductors. A Monte Carlo simulation study, *Physica Status Solidi B*, 1993, **175**(1), 15–56.
75 V. Joseph, J. Xia, A. A. Sutanto, V. Jankauskas, C. Momblona, B. Ding, K. Rakstys, R. Balasaravanan, C.-H. Pan, J.-S. Ni, S.-L. Yau, M. Sohail, M.-C. Chen, P. J. Dyson and M. K. Nazeeruddin, Triarylamine-Functionalized Imidazolyl-Capped Bithiophene Hole Transporting Material for Cost-Effective Perovskite Solar Cells, *ACS Appl. Mater. Interfaces*, 2022, **14**(19), 22053–22060.
76 K. Rakstys, M. Saliba, P. Gao, P. Gratia, E. Kamarauskas, S. Paek, V. Jankauskas and M. K. Nazeeruddin, Highly efficient perovskite solar cells employing an easily attainable bifluorenylidene–based hole–transporting material, *Angew. Chem.*, 2016, **128**(26), 7590–7594.
77 R. Durgaryan, J. Simokaitiene, A. Dabuliene, D. Volyniuk, O. Bezvikonnyi, V. Jankauskas, V. Matulis, D. Lyakhov, I. Klymenko, B. Schmaltz and J. V. Grazulevicius, N,N-di(4-methoxyphenyl)hydrazones of carbazole and phenothiazine carbaldehydes containing 4-methoxyphenyl groups as hole transporting materials, *Synth. Met.*, 2022, **287**, 117057.
78 (*a*) CCDC 2500277: Experimental Crystal Structure Determination, 2026, DOI: **10.5517/ccdc.csd.cc2pxr3h**; (*b*) CCDC 2455342: Experimental Crystal Structure Determination, 2026, DOI: **10.5517/ccdc.csd.cc2ndzln**.